BOTH SIDES CONTACTED SILICON SOLAR CELLS: OPTIONS FOR APPROACHING 26% EFFICIENCY

A. Richter[1], J. Benick[1], F. Feldmann[1], A. Fell[1], B. Steinhauser[1], J.-I. Polzin[1,2], N. Tucher[1], J. N. Murthy[1], M. Hermle[1], S. W. Glunz[1,2]
[1]Fraunhofer Institute for Solar Energy Systems ISE, Heidenhofstraße 2, 79110 Freiburg, Germany
[2]Laboratory for Photovoltaic Energy Conversion, Department for Sustainable Systems Engineering (INATECH), University of Freiburg, Emmy-Noether-Strasse 2, 79110 Freiburg, Germany
Corresponding author: armin.richter@ise.fraunhofer.de; Phone: +49-761-4588-5395

ABSTRACT: Recently, we demonstrated an efficiency of 25.8% for a both sides contacted silicon solar cell. These cells were realized on *n*-type Si featuring a boron-doped p^+ emitter at the front surface and a full-area tunnel oxide passivating contact (TOPCon) at the rear surface. In this work, we present a detailed electrical and optical loss analysis of this record cell in order to identify options to further improve the cell performance. Using a simulation-based electrical loss analysis, we are able to identify the main loss mechanisms and optimize e.g. the Si material (thickness, resistivity) as well as the front side emitter. Using an optical loss analysis as well as advanced optical simulations we also evaluated the potential of different light trapping schemes in order to increase the short-circuit current density. Altogether, an efficiency potential clearly beyond 26% is predicted, which is currently being investigated experimentally.
Keywords: silicon solar cells, TOPCon, power loss analysis, boron emitter, light trapping, device simulations

1 INTRODUCTION

Passivating contacts as tunnel oxide passivating contacts (TOPCon) [1] are considered to be one of the key technologies for the next generation of high efficiency silicon solar cell mass production and therefore intensive research activities are being carried out at research facilities as well as PV industries in this field. In fact, Trina Solar recently showed already impressive results on the mass production of i-TOPCon solar cells with a median efficiency of 23.0% [2]. These solar cells are fabricated on *n*-type silicon with a front side boron-doped emitter and TOPCon as a passivating rear contact, which is locally metallized to realize a bifacial solar cell design.

In order to study the ultimate efficiency potential of such kind of *n*-type Si solar cells with front-side boron-doped emitters and rear side TOPCon passivating contacts, we fabricate small-area solar cells with a quite similar solar cell design, with the difference that we apply a full-area metal contact to the TOPCon at the rear surface (i.e. a monofacial cell design) instead of local contacts. The fabrication of the solar cells includes various lab-type processes, e.g. photolithography-based structuring processes. This allows for optimized processes, e.g. for the front side contact formation including a selective emitter, beyond what is currently feasible using industrial-type technologies.

Recently, we have demonstrated that efficiency values up to 25.8% can be reached with these solar cells. In this work, we present a detailed electrical and optical loss analysis of the champion cell in order to identify the dominating loss mechanisms. Based on the results, we performed a detailed simulation study based on experimental data in order to investigate options to improve the cell performance beyond 26% by reducing the most significant power losses.

2 HIGH EFFICIENCY TOPCON SOLAR CELLS

2.1 Experimental solar cell results

Figure 1 shows a schematic cross section of the fabricated high-efficiency solar cells. They have a designated area of 2×2 cm^2 and were made of high-quality *n*-type float-zone (FZ) Si wafers with a resistivity of 1 Ω cm and a thickness of 200 µm. The front side features a diffused boron emitter with a sheet resistance of 300 Ω/sq. To reduce surface recombination losses at the front metal contacts, a heavily doped p^{++} emitter is located underneath the contacts. The rear surface features a full-area TOPCon/Ag contact. Details on the fabrication processes can be found in [3].

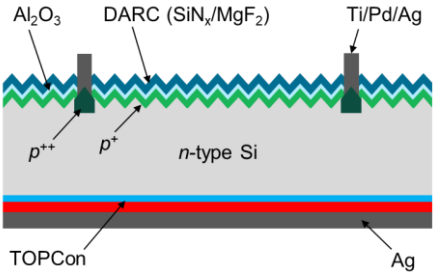

Figure 1: Schematic cross-section of the *n*-type Si solar cell with a front-side boron-doped emitter and full-area passivating rear contact (TOPCon).

Table 1: *I-V* parameters and *PFF* measured at the best cell under STC (designated area: 2×2 cm^2).

V_{OC} (mV)	J_{SC} (mA/cm^2)	*FF* (%)	*PFF* (%)	η (%)
724	42.9	83.1	85.6	25.8*

*Independently confirmed by Fraunhofer ISE CalLab

A confirmed efficiency of 25.8% has been achieved with these solar cells, which represents the highest efficiency reported for a *both-sides contacted* c-Si solar cell [4]. The cells benefit not only from a high open-circuit voltage V_{OC}, but also from a very high pseudo fill factor *PFF* of 85.6%, which allows for a very high fill factor *FF* level above 83%. A detailed analysis of the light trapping of the solar cell revealed that the random pyramids of these cells cause not only a light path enhancement by geometric optics but also by a relevant scattering effect [5]. This allows for a very high short-circuit current density J_{SC} of 42.9 mA/cm². In addition, the high J_{SC} level demonstrates that it is not necessarily an interdigitated back contact (IBC) solar cell design (like e.g. the record efficiency IBC solar cell from

Kaneka [4, 6]), which is required to realize highest J_{SC} values.

2.2 Electrical loss analysis

In order to quantify the power losses associated with electrical loss mechanisms, we established an accurate 3D full-area device simulation of a quarter of the complete solar cell including the perimeter region. The simulations were performed with Quokka3 [7], which is capable of solving such large-area simulations within a reasonable amount of time accurately. The power losses were derived from these simulations according to the free energy loss analysis (FELA) approach [8], which is implemented in Quokka3. The main simulation input parameters (listed in Table 2) are based on experimental measurements, e.g. with τ_{eff} measurements at symmetrically processed lifetime samples (with Al_2O_3-passivated p^+ emitter or TOPCon on *n*-type Si) for the J_0 values, or with four point probe measurements for the sheet resistance R_{sh} values. The optical model is based on a wavelength-dependent front surface transmission and a parameterization of the pathlength enhancement *Z*, as described in Ref. [9]. With this parameterization, the wafer thickness dependent *Z*, i.e. the J_{SC}, is correctly described, as required for the simulations described in Sec. 3.1. More details on the device simulation model and the measurements can be found in Ref. [3]. One variable parameter was the silicon bulk lifetime limitation, which was adapted in such a way that the solar cell *I-V* parameters were reproduced best, assuming an injection-independent lifetime limitation.

Table 2: Main simulation input parameters

Parameter	Value
Emitter sheet resistance $R_{sh,p+}$	300 Ω/sq
Emitter recombination ($J_{0e,p+,pass}$)	~7.5 fA/cm^2
Heavily doped emitter at front contact ($R_{sh,p++}$)	15 Ω/sq
Recombination at front contact ($J_{0e,p++,met}$)	~190 fA/cm^2
Front contact resistivity $\rho_{C,p++}$	0.25 mΩ cm^2
Recombination at TOPCon rear ($J_{0,TOPCon}$)	~1 fA/cm^2
Contact resistivity at TOPCon rear ($\rho_{C,TOPCon}$)	50 mΩ cm^2
Shunt resistance (R_{shunt})	4 kΩ cm^2

Table 3 shows the simulated *I-V* parameter for the best simulation configuration of the 25.8% cell. As can be seen, the *I-V* parameters are in quite good agreement with the measured values shown in Table 1. Thus, the 3D device model is considered as an accurate description of the fabricated cell and is as such well suited for the FELA. The resulting power losses are shown in Figure 2. They reveal that the main losses arise from Auger recombination in the high-quality FZ Si bulk and from the front side boron-doped emitter mainly due to recombination in the passivated region and lateral current transport towards the front side contact. Especially these two emitter losses sum up to an efficiency loss of almost 0.8%$_{abs}$. Note that although a very low J_{0e} value of ~7.5 fA/cm² was achieved for the 300 Ω/sq boron-doped emitter, a rather high power loss of 0.5%$_{abs}$ is still obtained for the emitter recombination. Another significant loss mechanism is the charge carrier recombination in the perimeter, which can, however, hardly be avoided for these small area solar cells embedded in a 10 mm diameter wafer.

At his point it is important to emphasize that the losses arising from the TOPCon rear (surface recombination, contact resistance) play only a minor role, because of its outstanding performance especially due to the extremely low $J_{0,TOPCon}$ value of only ~1 fA/cm².

Table 3: Simulated *I-V* parameters for the 25.8% solar cell configuration resulting from the 3D full-area simulations.

V_{OC} (mV)	J_{SC} (mA/cm^2)	*FF* (%)	η (%)
724	42.8	83.3	25.8

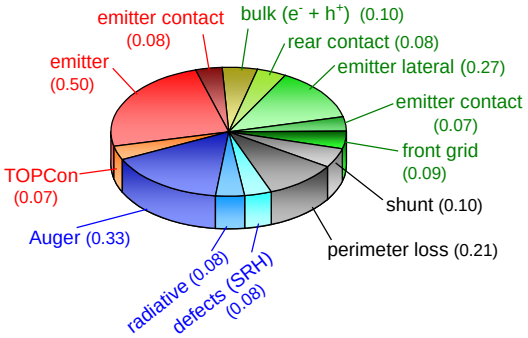

Figure 2: Electrical power losses resulting from the FELA based on the 3D full-area simulations. The losses in the silicon bulk are shown in blue, surface recombination losses in red, current transport losses in green and other losses in gray. The power losses in brackets are given in mW/cm² which is equivalent to an efficiency loss in %$_{abs}$.

2.3 Optical loss analysis

The optical loss analysis of the 25.8% cell is based on measured data of the external quantum efficiency *EQE* and the total reflectance *R*. Figure 3 shows the *EQE* data together with 1 – *R*. The total reflectance was separated into front surface reflectance and escape reflectance by a linear fit of *R* between 850 and 950 nm extrapolated to longer wavelengths, which is also shown Figure 3. The current losses associated with each optical loss mechanism were calculated via integration over the AM1.5g photon flux density. The results are also given in Figure 3. Note that the parasitic absorption or recombination losses (shown in red) were separated at a wavelength of 900 nm into front-side and rear-side losses.

The results reveal that there are only small contributions from front grid shading, front surface reflection, UV parasitic absorption and front recombination (the latter both cannot be separated from each other purely by the measurements). The main losses arise from escape reflection and IR parasitic absorption losses. These both losses are strongly affected by light trapping and especially the escape reflection can only be reduced to a certain amount because a very good light trapping will cause always also a substantial amount of escape reflection. At this point it is important to point out

that the full-area TOPCon/Ag rear contact enables already a very good light trapping with a pathlength enhancement factor Z = ~33 at a wavelength of 1200 nm.

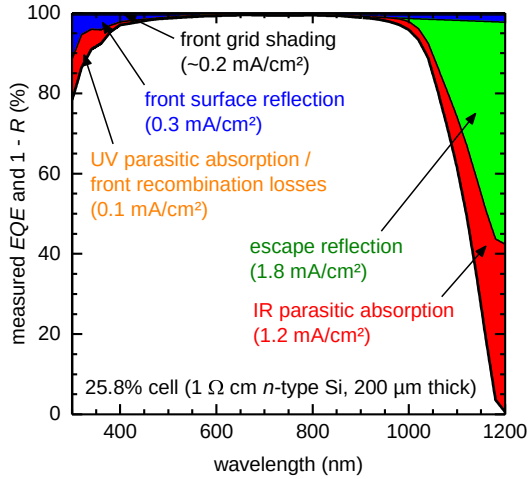

Figure 3: Optical loss analysis for the 25.8% cell based on measured *EQE* and reflectance data. The values in brackets are the current losses calculated from integration of the AM1.5g photon flux density.

3 SIMULATION BASED OPTIMIZATION

3.1 Base Material

Based on the 3D Quokka3 device simulation model used in the previous section for the electrical power loss analysis, we have performed a series of optimization simulations. First, we have varied the silicon base properties, i.e. the wafer thickness and resistivity, in order to identify its optimization potential. The results are shown in Figure 4a. The results indicate that, if the base resistivity is increased from 1 to 10 Ω cm for a 200 µm thick cell, the efficiency improves significantly by 0.2%$_{abs}$. An increase of the wafer thickness to 300 µm has only a minor influence. A decrease of the wafer thickness results in a decrease of the efficiency as well, in particular for the thinnest cell thickness of only 100 µm. For these cells, the gain in V_{OC} is overcompensated by the losses in J_{SC}.

Thus, to increase the efficiency, an increase of the wafer resistivity seems to be promising. However, high- resistivity silicon is also more sensitive to impurity contamination than low resistivity silicon [3]. To visualize this effect, we performed simulations (with the same simulation setup) as a function of the impurity concentration for 1 Ω cm and 10 Ω cm silicon, assuming the Shockley-Read-Hall (SRH) recombination properties of interstitial iron (Fe_i) [10] and interstitial chromium (Cr_i) [11]. The results are shown in Figure 4b. It can be clearly seen that for both, Fe_i and Cr_i, the high-resistivity (10 Ω cm) material shows the higher efficiency at low impurity concentrations, while at high impurity concentrations it suffers more from the impurity contamination than the low-resistivity material. This effect is more pronounced for Fe_i. However, the results also show that in general, Cr contamination is much more crucial for *n*-type Si than Fe contamination. In addition to Fe and Cr there are several other elements like Ti, Ni, Zn or Co, which are also very crucial for *n*-type Si [12, 13].

For the simulations shown in Figure 4a, we have assumed a SRH lifetime limitation of 44 ms (injection independent), which is the result of the electrical loss analysis described in Sec. 2.2, i.e. this assumption describes the experimental solar cell results best. If the cell is contaminated with Fe, this carrier lifetime limitation corresponds to a Fe_i concentration of 2×10^{10} cm^{-3}. This SRH lifetime limitation is high enough (i.e. the corresponding impurity concentration is low enough) to derive a significant benefit from increasing the wafer resistivity, as obtained from Figure 4a. A SRH lifetime limitation <12 ms, which would e.g. correspond to a Fe_i concentration of $>7\times10^{10}$ cm^{-3}, would result in the exact opposite: a low resistivity wafer would be beneficial, as we observed in one of our previous batches [3]. Note, however, that the type of contamination cannot be evaluated from this analysis, i.e. iron is only an assumption here.

Altogether, the results of Figure 4a show also that if the impurity contamination is low, the high efficiency level observed from the simulation results for >1 Ω cm resistivity and >150 µm wafer thickness is quite insensitive to a wide range of wafer resistivities and thicknesses, which is an important point for mass production, as a wide range of *n*-type Si materials can be used.

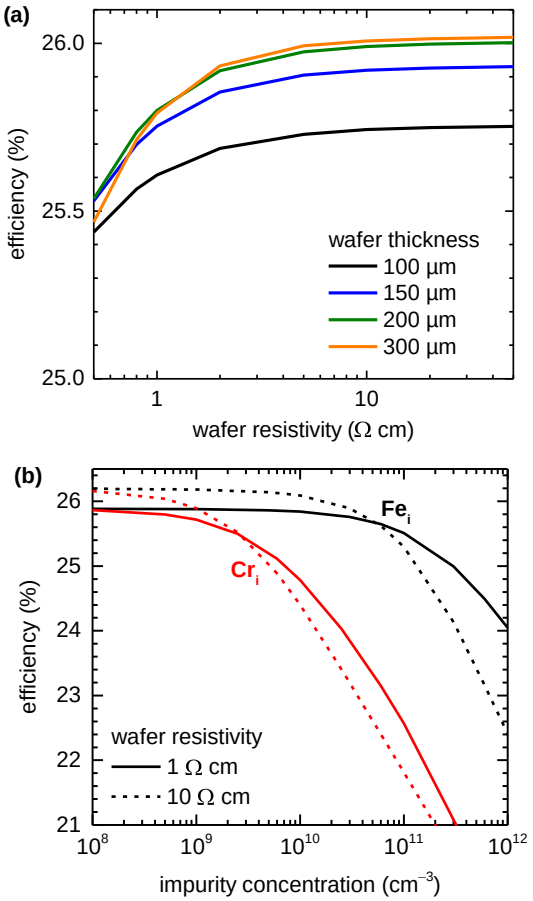

Figure 4: Simulated *I-V* parameters of the *n*-type Si solar cells shown in Figure 1 for a variation of wafer resistivity and thickness shown in (a) and an impurity concentration variation for interstitial Fe and interstitial Cr shown in (b). These simulations were performed with Quokka3 as described in Sec. 2.2 using the input parameters which describe the 25.8% solar cell best.

3.2 Emitter

The largest electrical power losses of the 25.8% cell originate from the emitter, mainly due to surface recombination and the lateral current transport towards the contacts. Emitter recombination losses can be reduced by reducing its doping concentration especially at the surface while exactly the opposite is required to achieve a high lateral conductivity. Thus, there is a trade-off which we studied also via the 3D device simulation. With respect to the lateral current transport, in particular the emitter sheet resistance and the distance between the contact fingers are of great importance, which thus have been varied in the device simulation.

For this kind of simulations, one needs to know the experimentally achievable range of emitter properties, i.e. the emitter recombination as a function of its sheet resistance. Therefore, we used data from Ref. [14], where recombination in form of J_{0e} was studied for different boron-diffused emitters on symmetrically processed lifetime samples with a random pyramids textured surface passivated with ALD Al_2O_3 capped with an ARC SiN_x layer deposited via PECVD. Figure 5 shows the J_{0e} values as a function of R_{sh}, including some additional data especially for R_{sh} > 200 Ω/sq, which were processed and analyzed as described in Ref. [14].[1] As can be seen, very low J_{0e} values of 3.5 fA/cm² were achieved on the 500±20 Ω/sq emitter, which is a quite promising result.

This $J_{0e}(R_{sh})$ data was used for the device simulation based emitter optimization. Figure 6 shows the results as a function of R_{sh} for three different finger pitches. For the two large pitches of 1.0 mm and 1.5 mm, we considered our high aspect ratio fingers shown Figure 7a, which are realized via photolithography-based lift-off of evaporated metal. These are the fingers we also used for the 25.8% cell. For the smallest pitch of 0.5 mm we assumed the advanced triangular-shaped fingers shown in Figure 7b, which we have already realized experimentally via photolithography-based metal lift-off. The difference of both fingers is that the triangular-shaped fingers have on the one hand a much lower cross-section area of only ~1/3, which causes a higher finger resistivity. On the other hand, the triangular-shaped fingers are considered to have a lower shading fraction as more light hitting the finger is reflected onto the solar cell. For the simulation we assumed a finger resistance based on the finger cross-section area and finger shading fractions of 70% for the high aspect ratio fingers and of 50% for the triangular-shaped fingers. Especially for our newly developed triangular-shaped fingers, this shading fraction is a rough estimation so far, and more characterization is necessary to get more confidence on the shading fraction assumed here.

The simulation results shown in Figure 6 reveal that an increase of R_{sh} from 300 Ω/sq (emitter of 25.8% cell) to 500 Ω/sq shows only a rather small efficiency gain if a pitch of 1.0 mm is used (pitch of 25.8% cell), because the gain in V_{OC} due to the substantially lower J_{0e} is almost entirely compensated by a lower *FF* due to higher current transport losses towards the front side contacts. For the higher pitch of 1.5 mm, an overall lower efficiency level is observed because lateral transport losses dominate over all the other effects. For the 0.5 mm pitch combined with the triangular-shaped fingers, however, a rather high efficiency gain of ~0.4%$_{abs}$ is predicted, as indicated by the arrow. As such, these triangular-shaped fingers combined with a significantly reduced finger pitch seems to be a promising approach to increase the efficiency substantially.

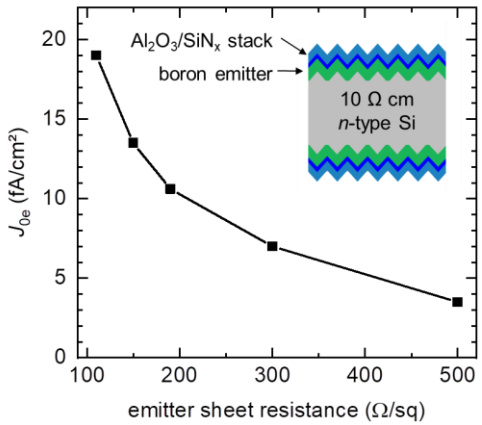

Figure 5: Experimental J_{0e} results as a function of the sheet resistance. The results were obtained from symmetrically processed lifetime samples with a random pyramids textured surface and an ALD Al_2O_3 passivated boron-doped emitter. Some of the results are from Ref. [14].

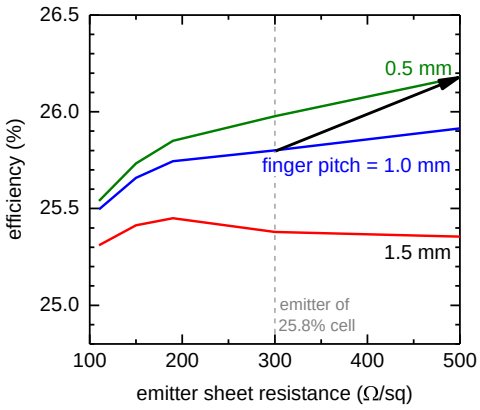

Figure 6: Simulated *I-V* parameters of the *n*-type Si solar cells shown in Figure 1 as a function of the emitter sheet resistance for three different finger pitches. The properties of the high aspect ratio fingers shown in Figure 7a were assumed for simulations with 1.0 mm and 1.5 mm, while the triangular-shaped fingers shown in Figure 7b were considered for the small pitch of 0.5 mm.

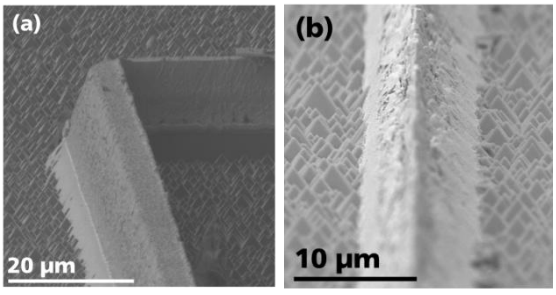

Figure 7: (a) SEM image of our high aspect ratio fingers, used for the 25.8% cell. (b) SEM image of our newly developed triangular-shaped fingers. Both fingers are realized via photolithography-based lift-off of evaporated metal.

[1] The ALD Al_2O_3 films of the additional emitters was deposited at 180°C instead of 230°C as reported in Ref. [14].

3.3 Light trapping

The optical loss analysis revealed high losses arising from parasitic IR absorption and escape reflection, although the full-area Ag contact at the rear combined with the front side texture has already a quite good light trapping. In order to investigate if the IR light trapping performance can still be improved, we performed optical simulations using OPTOS [15], which allows to consider the scattering at the random pyramids (RPs) [5] as well as absorption effects in local metal contacts. Three different rear-side light trapping schemes were simulated: (i) planar/Ag (design of 25.8% cell), (ii) planar/SiO_x/Ag and (iii) RPs/SiO_x/Ag. The thickness of the SiO_x was 150 nm. The TOPCon layer at the rear surface (between the silicon base and the mirror) was not considered in the simulations, because it has only a very minor influence on the results especially as it is with ~15 nm very thin and thus, no significant free carrier absorption is expected. The front-side was identical for the three different variations and consists of an RPs textured surface coated with the Al_2O_3 passivation layer and a double layer ARC (SiN_x/MgF_2). In addition, the parasitic absorption effects due to the front side contacts (~1% area fraction) are already considered, while local rear contacts are not considered in this simulation.

The simulation results are shown in Figure 8. The results indicate that there is only a small J_{SC} gain of 0.2 mA/cm² for the SiO_x/Ag mirror on a planar rear, while a significantly higher gain of 0.5 mA/cm² is predicted for the SiO_x/Ag mirror on the textured rear. As TOPCon shows an extremely high passivation quality not only on planar surfaces, but also on RPs textured surfaces with implied V_{OC} values of 734 mV [16], a textured rear in combination with the SiO_x/Ag mirror seems to be quite promising. The application of such SiO_x/Ag mirrors requires, however, local contacts to the TOPCon instead of a full-area contact as utilized for the 25.8% cell. These local contacts require further optimization with respect to the metallized area fraction, distance between the local contacts as well as the influence of the contact size on the light trapping. Results regarding these optimizations for *n*-type Si solar cells with the SiO_x/Ag mirror and local contacts to the TOPCon will be published elsewhere.

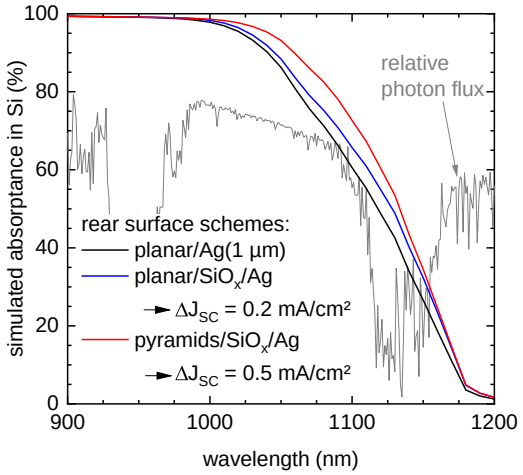

Figure 8: Optical simulations performed with OPTOS for different light trapping schemes on the rear surface. The J_{SC} gain with respect to the planar/Ag rear is also given. For comparison, the relative AM1.5g photon flux spectrum is also plotted.

5 SUMMARY

We have studied the electrical and optical losses of our 25.8% champion cell featuring a boron-doped front side emitter and a full-area TOPCon rear contact. The electrical power loss analysis indicates that the main losses arise from Auger recombination in the silicon base and from the emitter mainly due to recombination in the passivated region and lateral current transport towards the front side contacts. Accurate 3D full-area device simulations predict an efficiency improvement of $0.2\%_{abs}$ for optimized material (resistivity and thickness), when assuming the same estimated level of SRH defects. With an optimized high resistivity emitter combined with our newly developed triangular-shaped front fingers and a reduced finger pitch, an efficiency improvement of $\sim 0.4\%_{abs}$ is predicted. Optical simulations indicate a J_{SC} improvement of 0.5 mA/cm², if a textured rear is combined with a SiO_x/Ag mirror. For an accurate efficiency potential prediction of this advanced light trapping, there is a further analysis required because in this configuration the full-area TOPCon/Ag contact used for the 25.8% needs to be replaced by local contacts. Based on first experimental results, we see also a high chance that the advanced light trapping improves the efficiency as well.

Altogether, a clear efficiency potential beyond 26% is predicted by the device simulations including all synergy effects and all the discussed improvements are currently implemented in new solar cell batches, to study the efficiency potential experimentally.

ACKNOWLEDGEMENTS

The authors want to thank the colleagues from the Fraunhofer ISE **ETA***lab*, who contributed to this work, in particular S. Seitz, A. Leimenstoll, F. Schätzle, N. Brändlin, and H. Steidl for the processing of the champion cell batch, S. Seitz and N. Sherkat for the contribution to the development of photo-lithography processes, and F. Martin und E. Schäffer for measurements. This work was partially funded by the German Federal Ministry for Economic Affairs and Energy under grant No. 0325827B (26+).

REFERENCES

[1] F. Feldmann, M. Bivour, C. Reichel, M. Hermle, and S. W. Glunz, "Passivated rear contacts for high-efficiency n-type Si solar cells providing high interface passivation quality and excellent transport characteristics," *Sol. Energy Mater. Sol. Cells*, vol. 120, p. 270, 2014.

[2] Y. Chen *et al.*, "Mass production of industrial tunnel oxide passivated contacts (i-TOPCon) silicon solar cells with average efficiency over 23% and modules over 345 W," *Prog Photovolt Res Appl*, 2019.

[3] A. Richter *et al.*, "n-Type Si solar cells with passivating electron contact: Identifying sources for efficiency limitations by wafer thickness and resistivity variation," *Sol. Energy Mater. Sol. Cells*, vol. 173, p. 96, 2017.

[4] M. A. Green *et al.*, "Solar cell efficiency tables (version 54)," *Prog Photovolt Res Appl*, vol. 27, no. 7, p. 565, 2019.

[5] O. Höhn, N. Tucher, A. Richter, M. Hermle, and B. Bläsi, "Light scattering at random pyramid

textures: Effects beyond geometric optics," *AIP Conf. Proc.* (SiliconPV 2018), vol. 1999, p. 30002, 2018.

[6] K. Yoshikawa *et al.*, "Silicon heterojunction solar cell with interdigitated back contacts for a photoconversion efficiency over 26%," *Nat. Energy*, vol. 2, p. 17032, 2017.

[7] A. Fell, J. Schön, M. C. Schubert, and S. W. Glunz, "The concept of skins for silicon solar cell modeling," *Sol. Energy Mater. Sol. Cells*, vol. 173, p. 128, 2017.

[8] R. Brendel, S. Dreissigacker, N.-P. Harder, and P. P. Altermatt, "Theory of analyzing free energy losses in solar cells," *Appl. Phys. Lett.*, vol. 93, no. 17, p. 173503, 2008.

[9] A. Fell, K. R. McIntosh, K. C. Fong, "Simplified device simulation of silicon solar cells using a lumped parameter optical model," *IEEE J. Photovoltaics*, vol. 6, no. 3, 611, 2016.

[10] A. A. Istratov, H. Hieslmair, and E. R. Weber, "Iron and its complexes in silicon," *Appl. Phys. A*, vol. 69, no. 1, p. 13, 1999.

[11] J. Schmidt, R. Krain, K. Bothe, G. Pensl, and S. Beljakowa, "Recombination activity of interstitial chromium and chromium-boron pairs in silicon," *J. Appl. Phys.*, vol. 102, no. 12, p. 123701, 2007.

[12] A. Richter, J. Benick, A. Fell, M. Hermle, and S. W. Glunz, "Impact of bulk impurity contamination on the performance of high-efficiency n -type silicon solar cells," *Prog Photovolt Res Appl*, vol. 24, no. 10, p. 1319, 2018.

[13] J. Schmidt *et al.*, "Impurity-Related Limitations of Next-Generation Industrial Silicon Solar Cells," *IEEE J. Photovoltaics*, vol. 3, no. 1, p. 114, 2013.

[14] A. Richter, J. Benick, and M. Hermle, "Boron emitter passivation with Al_2O_3 and Al_2O_3/SiN_x stacks using ALD Al_2O_3," *IEEE J. Photovoltaics*, vol. 3, no. 1, p. 236, 2013.

[15] N. Tucher *et al.*, "3D optical simulation formalism OPTOS for textured silicon solar cells," *Opt. Express*, vol. 23, no. 24, A1720, 2015.

[16] J.-I. Polzin, F. Feldmann, B. Steinhauser, M. Hermle, and S. Glunz, "Realization of TOPCon using industrial scale PECVD equipment," *AIP Conf. Proc.* (SiliconPV 2018), vol. 1999, p. 40018, 2018.